Applied Catalysis B: Environmental 239 (2018) 154–167

Contents lists available at ScienceDirect

Applied Catalysis B: Environmental

journal homepage: www.elsevier.com/locate/apcatb

Mono- and bimetallic nano-Re systems doped Os, Mo, Ru, Ir as nanocatalytic platforms for the acetalization of polyalcohols into cyclic acetals and their applications as fuel additives

Maciej Kapkowski[a,*], Judyta Popiel[a], Tomasz Siudyga[a], Marzena Dzida[a], Edward Zorębski[a], Małgorzata Musiał[a], Rafał Sitko[a], Jacek Szade[b], Katarzyna Balin[b], Joanna Klimontko[b], Maciej Zubko[c], Jaroslaw Polanski[a,*]

[a] Institute of Chemistry, University of Silesia, Szkolna 9, 40-006 Katowice, Poland
[b] Institute of Physics, University of Silesia, 75 Pułku Piechoty 1A, 41-500 Chorzów, Poland
[c] Institute of Materials Science, University of Silesia, 75 Pułku Piechoty 1A, 41-500 Chorzów, Poland

ARTICLE INFO

Keywords:
Re, Ru, Os, Mo, Ir nanoparticles
Heterogenous catalysis
Cyclic acetals
Fuel additives
Silica supported nanorhenium

ABSTRACT

We report here that the Re/SiO_2 catalyst can be a suitable low-cost catalyst for processing polyols into acetals in solvent-free conditions with a high conversion rate and selectivity up to 100% in mild conditions. During a complex investigation, we broadly tested the blending potential of the acetals that were formed by measuring properties such as density, viscosity, isentropic compressibility, isobaric thermal expansion, cetane number and other parameters of both the crude additives and the blends that were prepared with petroleum diesel oil. The results indicate that the investigated acetals can generally be used for blending with petroleum diesel oil in order to obtain the valuable biofuels that are in great demand in the contemporary transportation industry due to the regulatory restrictions that have been introduced in order to protect the environment.

1. Introduction

Glycerol is a polyalcohol that is available in large amounts as a by-product of the hydrolysis of fats into fatty acids, in particular, in the production of biodiesel from vegetable oils. As a tri-carbon C_3 alcohol, glycerol is an attractive raw material for the synthesis of various chemicals that have a higher economic value [1]. Processing this non-toxic, colorless, viscous, odorless, hygroscopic alcohol, whichmixes without restrictions with water and ethanol [1] can include dehydration [2–6], chlorination [7–9], oxidation [10–13], reforming [14–16], hydrogenation [17–19], esterification or etherification [20,21]. From an industrial point of view, glycerol can be an important crude material for the production of fuel additives (tert-butyl derivatives, cyclic acetals, methyl and ethyl esters), bulk solvents (propylene glycol, ethylene glycol, methanol) as well as important industrial compounds (acrolein, epichlorhydrin, hydroxypropionic acid) [1,22]. In addition, the steady demand for oxygenates C_3 (lactic acid, glyceraldehyde, dihydroxyacetone), the source of which may be glycerol, indicates an attractive direction in the use of its surplus. Usually, the above-mentioned processes are based on a transition metal (Au, Pd, Pt, Re, Ru, Ni, Zr, W, Cu, Mo) catalysis [1–22]. Alternative biotechnologies appear to be economically controversial due to the considerable complications of the larger-scale processing of micro-organisms [23–25].

Regulatory issues are important motivations for the production of glycerol-based fuel additives. Shrinking fossil fuel resources and environmental degradation have resulted in the need to find alternative solutions to ensure energy supplies in the future. Therefore, various legal regulations have been designed to force industry to develop new blended fuels that are based on biocomponents. The market for biofuels is constantly expanding due to their ever-increasing use in various branches of the transport sector, which has seen continuous growth in recent years. For example in 2013, global biodiesel production reached a ceiling of more than 110 billion liters and it is predicted that it will grow to about 141 billion liters by 2022 [26]. Compared to diesel, biodiesel, which has similar properties, is considered to be a more favorable alternative because it is renewable, biodegradable and non-toxic [27,28]. In turn, the production of biodiesel generates large amounts of glycerol, which due to its decomposition and polymerization, which causes engine problems cannot be used directly for blending fuels. This is the main reason that the net price of 1 ton of technical

* Corresponding authors.
E-mail addresses: maciej.kapkowski@us.edu.pl (M. Kapkowski), polanski@us.edu.pl (J. Polanski).

https://doi.org/10.1016/j.apcatb.2018.07.071
Received 22 May 2018; Received in revised form 19 July 2018; Accepted 27 July 2018
Available online 29 July 2018
0926-3373/

glycerol ranged between € 280–300 in 2017 and it is projected that prices will continue to fall. Glycerol functionalization, for example, to cyclic acetals, esters or ethers not only allows its utilization, thereby increasing its economic value as a raw material, but also significantly improves its fuel-like parameters. In this context, the improvement of viscosity, density, ignition point, octane or cetane number or the reduction of particulate emissions have been investigated [27–31]. From a chemical point of view, the utilization of waste glycerol is the main reason for using this material in blending fuels. However, fuel additives can also prevent the abrasion of engine properties, for example, in piston engines that have a spark ignition; bushings, connecting rods and crankshaft bearings, while in diesel engines, it can reduce injector nozzle contamination and engine noisiness. Furthermore, a well-selected fuel composition not only reduces the amount of harmful engine "stings", but also reduces the formation of gums and deposits, thereby permitting the longer storage of a fuel [32].

The cyclic acetals that are obtained from polyols can provide useful fuel additives. Currently, the synthesis of these compounds require the use of strong inorganic acids (H_2SO_4, HCl, HNO_3) or organic acids (dichloroacetic acid, p-toluenesulfonic acid) and organic solvents (toluene, dioxane, tetrahydrofuran, cyclohexane, dichloromethane) [22,30,33]. Usually, the reactions are conducted in an inert gas atmosphere in a temperature range of 70–110 °C, which yields a conversion rate of 60–95% depending on the method that is used [34–37]. Catalytic methods are based on metals (Fe), transition metal complexes, e.g. Cu, Ir [36,38] or metal oxides (ZrO_2) that are supported on silica or aluminosilicates [34,35], surface-modified activated carbon [37] or polymeric fibers [39]. Other solutions include the use of low-temperature catalysts such as an SnO_2 doped with W or Mo [30], ionic fluids [40] or the Amberlyst ion-exchange resin [41].

There are a large number of reports in the patent literature regarding the use of (2,2-dimethyl-1,3-dioxolan-4-yl)methanol (solketal), which is the final product of the acetylation of glycerol as an additive that is used to improve the octane number of gasoline and the properties of lubricants that have a high viscosity [42–46]. In research on the use of solketal and other 1,3-dioxolanes, authors have suggested that it can be blended into a fuel up to 5% by weight because blending above this limit is prevented by the delamination effect [32]. Solketal's limited miscibility inspired the use of various acetal mixtures to produce the desired physico-chemical fuel-like properties of blended products.

This article focuses on ecological and selective catalytic methods for the synthesis of low-molecular weight cyclic acetals from polyols (ethylene glycol, propylene glycol, glycerol) and acetone (Scheme 1). The synthesis was based on the heterogeneous catalysis on nanometallic transition metals. In the search for novel methods for the blending the so-called I and II generation fuels and biofuels [47–51], we investigated the range of the applicability of cyclic acetals as potential additives for two types of biodiesel oil by determining the basic performance parameters of the prepared mixtures. This included density, kinematic viscosity, speed of sound, isentropic compressibility, isobaric thermal expansion and cetane number.

2. Experimental

2.1. Preparation of mono- and bimetallic Re, Os, Mo, Ru, Ir NPs on sol-gel silica

A series of mono- or bimetallic Re silica-supported nanocatalysts that had been doped with Os, Mo, Ru or Ir were prepared according to an optimized procedure. This carrier is obtained using the Stöber method [52] with tetraethyl orthosilicate (TEOS), which is added to a mixture of methanol and an aqueous ammonia solution [53]. The mixture was sonicated, then concentrated, dried and reduced under hydrogen at 500 °C. For the general procedure, a solution of anhydrous methanol (99.8% Sigma Aldrich, St. Louis, MO, USA) 1500 mL and 528 mL of 25% wt. of an ammonia solution (Chempur) were mixed. After 10 min of stirring, 100 mL of tetraethyl orthosilicate (99.0% Sigma Aldrich, St. Louis, MO, USA) was added to the reaction mixture, which was then stirred for 3 h at room temperature. The colloidal silica suspension was centrifuged and washed with distilled water in an ultrasound bath until a neutral pH was achieved (pH was determined using universal indicator paper). A solution containing Re and/or an Os, Mo, Ru or Ir precursor (Table S1, Supplementary materials) in deionized water (10 mL) was added dropwise into the obtained carrier, i.e. colloidal silica and stirred for 30 min. Next, it was dried at 60–90 °C for about 4 h in the dark, ground and sieved. The reduction was conducted in an oven under hydrogen atmosphere at 500 °C for 4 h.

2.2. Methods for the characterization of the catalysts

The chemical analysis was performed using an energy-dispersive X-ray fluorescence (EDXRF) spectrometer – Epsilon 3 (Panalytical, Almelo, The Netherlands) with an Rh target X-ray tube, which was operated at a max. voltage of 30 keV and a max. power of 9 W. The spectrometer is equipped with a thermoelectrically cooled silicon drift detector (SDD) with an 8 µm Be window and a resolution of 135 eV at 5.9 keV. The quantitative analysis was performed using Omnian software based on the fundamental parameter method and the following measurement conditions: 5 kV, 300 s counting time, helium atmosphere for Si determination and 30 kV, 120 s counting time, air atmosphere and a 100 µm Ag primary beam filter for Re, Mo and Os. The current of the X-ray tube was fixed to not exceed a dead-time loss of ca. 50%.

In order to determine the structural features of the samples that were studied, X-ray diffraction experiments (XRD) were performed. A high-resolution PANalytical Empyrean diffractometer equipped with a PIXcel detector was used with Cu K_α radiation (40 kV, 30 mA). Data was collected in the 5°–140° 2θ range with 0.0131° steps. The phase analysis was performed using the "X'Pert High Score Plus" computer program using data from the ICDD PDF-4 database.

The transmission electron microscopy (TEM) observations were performed using a JEOL high resolution (HRTEM) JEM 3010 microscope working at 300 kV accelerating voltage and equipped with a Gatan 2k × 2k Orius™ 833SC200D CCD camera. The samples were suspended in isopropanol and the resulting materials were deposited on a Cu grid that had been coated with an amorphous carbon film that was standardized for the TEM observations.

The resulting preparations of silica-supported mono- and bimetallic catalysts were examined using X-ray photoelectron spectroscopy (XPS) with a Prevac/VGScienta photoelectron spectrometer. Monochromatic AlKα x-ray radiation ($h\nu$ = 1486.7 eV) was used to obtain the photoelectron spectra of the core levels of specific elements. The structure of the XPS multiplets that were obtained was analyzed using the Multipak program from Physical Electronics.

2.3. Polyols acetalization procedure with acetone

A mono- or bimetallic Re, Ru, Os, Ir or Mo heterogeneous nanocatalyst (50 mg, 1.3–5.2 µmol nanometal/s) was suspended in a mixture of 3.86 mL (0.05 mol) acetone (99.0% Avantor) and 0.28 mL (0.005 mol) ethylene glycol (99.0% Across Organics) or 0.37 mL (0.005 mol) propylene glycol (99.0% Across Organics) or 0.37 mL (0.005 mol) glycerol (99.5% Fisher BioReagents® – Glycerol For Molecular Biology, Fisher Scientific, Waltham, MA, USA) using ultrasonic cleaner at room temperature for 10 min (RK 52 H, Bandelin Electronics, 35 kHz). The reagent solution was stirred at 200 rpm in a sealed tube (septa system), which was placed in a thermostated oil bath at 55 °C for 1 h. The resulting reaction mixture was centrifuged and decanted. The supernatant was dissolved into deuterium oxide and analyzed using ^1H and ^{13}C NMR. Additionally, the 2D COSY and HMQC methods were used to identify and quantify the products. The spectra were recorded on a Bruker Avance (500 MHz, ^1H, 126 MHz ^{13}C)

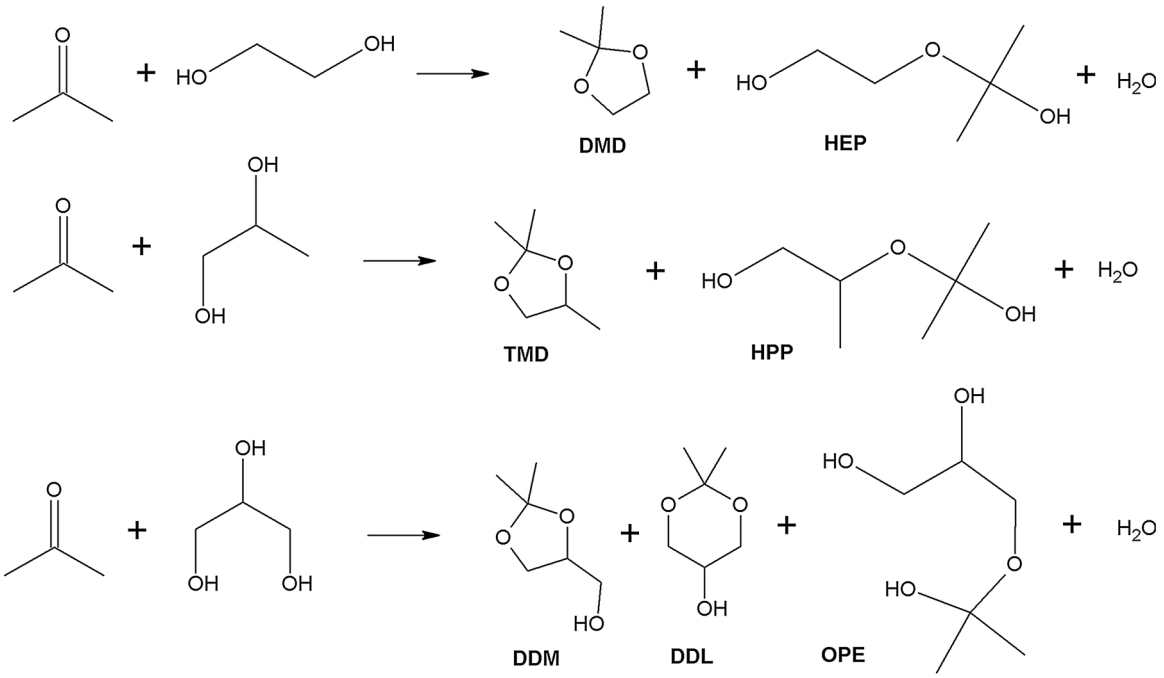

Scheme 1. Possible reaction products for the direct polyol (ethylene glycol, propylene glycol and glycerol) acetalization with acetone. Individual abbreviations means: DMD – 2,2-dimethyl-1,3-dioxolane, HEP – 2-(2-hydroxyethoxy)propan-2-ol, TMD – 2,2,4-trimethyl-1,3-dioxolane, HPP – 2-(2-hydroxypropan-2-yloxy) propan-1-ol, DDM – (2,2-dimethyl-1,3-dioxolan-4-yl)methanol – (solketal), DDL – 2,2-dimethyl-1,3-dioxane-5-ol, OPE – 3-(2-oxidanylpropan-2-yloxy)propane-1,2-diol.

spectrometer at room temperature. The signal from the water was suppressed using 90 water-selective pulses (zggpwg). NMR analyses are much clearer if high purity alcohols are used as the reagents, which limited the possibility of using this type of analysis here.

GC-FID chromatography was also used as a complementary technique to confirm presence of cyclic acetals that were obtained. The composition of a product was determined by gas chromatography using a gas chromatograph with a flame ionization detector FID (capillary column 60 m × 0.25 mm with DB-Wax as the stationary phase, inlet temperature 250 °C, injection volume 1.0 µl, carrier gas He, gas flow 10 $dm^3 h^{-1}$, column temperature 150 °C, and detector temperature of 275 °C). Eqs. (1)–(4) were used to calculate the conversion rate, product selectivity, yield and TON, respectively. Selected NMR and GC-FID spectra with retention time, chemical shifts for the starting materials and products are presented in the Supplementary material, Figs. S1A–E, S2A–E and S3A–E.

$$Conversion\ (\%) = \frac{(initial\ moles\ of\ alcohol - final\ moles\ of\ alcohol)}{initial\ moles\ of\ alcohol} \times 100 \quad (1)$$

$$Selectivity\ of\ products\ (\%) = \frac{percentage\ amount\ of\ product\ formed}{the\ total\ percentage\ of\ all\ product\ formed} \times 100 \quad (2)$$

$$Yield\ (\%) = \frac{conversion\ of\ alcohol\ x\ selectivity\ of\ desired\ product}{100} \quad (3)$$

$$TON = \frac{\alpha \cdot n_{sub}}{n_{met}} \quad (4)$$

Where n_{sub} – total number of moles of the substrate, n_{met} – number of moles atoms of the nanometal/s, α – system conversion rate.

2.4. Polyols acetalization procedure with other ketones

A monometallic Re heterogeneous nanocatalyst (50 mg, 2.7 µmol Re) was suspended in a mixture of 4.49 mL (0.05 mol) 2-butanone (99.0% Sigma Aldrich) or 5.39 mL (0.05 mol) 3-propanone (98.0% Acros Organics) with one of the polyols 0.28 mL (0.005 mol) ethylene glycol (99.0% Across Organics) or 0.37 mL (0.005 mol) propylene glycol (99.0% Across Organics) or 0.37 mL (0.005 mol) glycerol (99.5% Fisher BioReagents® – Glycerol For Molecular Biology, Fisher Scientific, Waltham, MA, USA) using ultrasonic cleaner at room temperature for 10 min (RK 52 H, Bandelin Electronics, 35 kHz). The reagent solution was stirred at 200 rpm in a sealed tube (septa system), which was placed in a thermostated oil bath at 55 °C for 1 h. The resulting reaction mixture was centrifuged and decanted. The post-reaction mixture was analyzed as was described in paragraph 2.3.

2.5. Large-scale tests and separation of the products from the post-reaction mixture

HZSM-5 zeolite (Sigma Aldrich) or Amberlyst-36 (Sigma Aldrich) or a 1.0% Re/SiO_2 catalyst (500 mg) were suspended in a mixture of 386 mL (5 mol) acetone (99.0% Avantor) and 28 mL (0.5 mol) ethylene glycol (99.0% Across Organics) or 37 mL (0.5 mol) propylene glycol (99.0% Across Organics) or 37 mL (0.5 mol) glycerol (99.5% Fisher BioReagents® – Glycerol For Molecular Biology) using ultrasonic cleaner at room temperature for 10 min (RK 52 H, Bandelin Electronics, 35 kHz). The reagent solution was stirred at 200 rpm in a reflux, which was placed in a thermostated water bath at 55 °C for 1 h. The resulting reaction mixture was centrifuged and decanted. The post-reaction mixture was analyzed as was described in paragraph 2.3.

The 2,2-dimethyl-1,3-dioxolane or 2,2,4-trimethyl-1,3-dioxolane was separated from post-reaction mixture using combined methods that were based on the physico-chemical properties of the reagents and products. In the first stage, after separating the catalyst by centrifugation, acetone was distilled under reduced pressure (200–150 mBa) at a low temperature (20–22 °C) to a final volume of ca. 60 mL. In the

second stage, about 60 mL of distilled water was added to the mixture of the distillate and 25–30 g of NaCl. After 5 min, the separation of two layers was observed; the upper layer was the product. The product was separated in a separatory funnel. The separated product was then dried by the addition of 5 g of Na_2SO_4.

Solketal – (2,2-dimethyl-1,3-dioxolan-4-yl)methanol was separated from the post-reaction mixture *via* the evaporation of the excess acetone under reduced pressure (200–150 mBa) at 20–30 °C. After the acetone was removed, the water from the solketal was distilled under nitrogen atmosphere and reduced pressure (40–50 mBa) at 60 °C for 45 min. The product was then dried over 5 g of Na_2SO_4.

2.6. Measuring physico-chemical properties of the cyclic acetals

2.6.1. Density and speed of sound

The density and speed of sound were measured using a vibrating tube densimeter (Anton Paar model DMA5000M) and sound analyzer (Anton Paar model DSA5000M), respectively. The uncertainty of the density measurements was estimated to be less than $\pm 5 \times 10^{-2}$ kg m^{-3} and the repeatability less than $\pm 5 \times 10^{-3}$ kg m^{-3}. The uncertainty of the speed of sound measurements was estimated to be less than $\pm$ 0.5 m s^{-1}.

2.6.2. Viscosity

The kinematic viscosity of the samples was measured using a pre-calibrated Ubbelohde-type glass capillary viscometer (Schott, Mainz, Germany) with a capillary constant of 0.03086 mm^2 s^{-2}. The capillary viscometer was immersed vertically in a thermostat fluid that was circulating in a glass cylinder. A cascade arrangement of two bath-type laboratory thermostats, which were equipped with a PI temperature controller (Unipan, Warsaw, Poland), allowed the temperature of the sample to be kept within 0.01 °C. The temperature was measured using a NIST-certified Pt-100 probe and an Ertco-Hart digital thermometer (Hart Scientific, American Fork, UT, USA). In this study, the measurements were performed at least in triplicate in each case and no Hagenbach-Couette correction was needed because of the large flow times. The scatter of the results from multiple measurements indicated an experimental uncertainty of ± 1%.

2.6.3. Water content

The water content was determined using a TitroLine 7500 Trace Karl Fischer Coulometric Titrator, which has a nominal detection limit of 1 ppm. The calibration and characteristics of the work of the Karl Fischer Coulometric Titrator were performed as described by Skowronek et al. [54].

The other physico-chemical parameters of the two tested diesels and their mixtures with cyclic acetals are collected in the Supplementary materials as certified tests (Tables S2–S7, Supplementary materials).

3. Results and discussion

3.1. Preparation and structure of the catalysts

The EDXRF spectra of the new catalysts had a high intensity Si Kα peak at 1.74 as well as several peaks of the Re, Mo and Os nanoparticles. The EDXRF spectrum of the Re/SiO_2 had several peaks of the L series that corresponded to the L3 edge (Re Lα and Ll at 8.65, 7.60 keV), the L2 edge (Re Lβ1 and Lγ1 at 10.01, 11.69 keV) and the L1 edge (Lγ2,3 at 12.08 keV). The EDXRF spectrum of the Mo/SiO_2 had two high intensity Mo Kα and Mo Kβ peaks at 17.48 and 19.61 keV. The spectra of the catalysts that contained the Re and Os nanoparticles (ReOs/SiO_2) had peaks of both Re (Lα, Lβ1 and Lγ1 at 8.65, 10.01 and 11.69 keV) and Os (Lα, Lβ1 and Lγ1 at 8.91, 10.35 and 12.09 keV). The EDXRF spectra of Re/SiO_2, Mo/SiO_2 and ReOs/SiO_2 catalysts are shown in Fig. 1 and the quantitative analysis is presented in Table 1.

The XRD results of the monometallic Re silica-supported nanocatalysts that had been doped with Os, Ru or Ir are presented in Fig. 2A, B, which show the X-ray diffraction patterns in the range of the 2θ angle from 10 to 100°. It clearly shows the peaks that can be attributed to the pure hexagonal ($P6_3/mmc$) phases of the Re, Ru and Os NPs and the considerably weaker lines of the cubic ($Fm\bar{3}m$) phase of the Ir NPs. The molybdenum Mo nanoparticles were below the detection limit for the XRD technique. The broad peak at the low angle range was due to the silica. It can be clearly seen that the experimental profiles of the Os NPs are broader than those from the other nanomaterials, thereby suggesting that the Os nanoparticles are very small.

The Scherrer equation was used to estimate the average size of the crystalline particles. Their size was estimated from the strongest diffraction lines ($2\theta_{101} \sim 43°$ for the Re and Os NPs, $2\theta_{101} \sim 44°$ for the Ru NPs, $2\theta_{111} \sim 40.5°$ for the Ir NPs and $2\theta_{111} \sim 37.5°$ for the Mo NPs) and values from about 3 nm for the Os NPs to about 10–11 nm for the Ru NPs were obtained. The lattice parameters of the investigated nanomaterials (calculations using the "Chekcell v.4" computer program) as well as the average crystallite size that were determined using the XRD method are listed in Table 2.

Fig. 2B presents the X-ray diffraction patterns of the 1.0% ReRu (1:1)/SiO_2, 1.0% ReOs(1:1)/SiO_2 and 1.5% ReMo(2:1)/SiO_2 catalysts. These were compared with the 1.0% Re/SiO_2 specimen. The broad peak at the low angle range was due to the silica. Since the Re, Ru and Os NPs had the same primitive hexagonal structure and their lattice parameter only differed slightly, an overlapping of the diffraction lines was observed. Profile fitting was performed in order to determine the crystallite size and lattice parameters of the XRD peaks (Fig. 2C). The calculated values are listed in Table 2. The smallest crystallite sizes were those for the Os NPs for both the mono- and bimetallic systems. However, some of the nanoparticles were below the detection limit of the XRD method.

The structure of the selected XPS core levels of the metallic components was analyzed with respect to its chemical state and the possible formation of alloys. Due the limited inelastic mean free path of photoelectrons, the analysis depth was limited to about 2–4 nm. The structure of the Re 4f level in a monometallic system is presented in Fig. 3a. The experimental spectrum was fitted using three spin-orbit doublets. The position of the most intense doublets revealed a specific metallic state of the binding energy that was shifted towards a higher binding energy with the respect to the pure metal by a few tens of eV. Moreover, the line-width was much larger than that reported for a bulk metal [PHI Handbook, NIST database]. Such a shift and increased linewidth were reported for metal nanoparticles which were assigned to quantum confinement and a distribution of nanoparticle sizes [55]. The two doublets that fit in the binding energy range of 43–50 eV can be attributed to the oxidized state of Re. While the second doublet apparently originated from ReO_2 and/or ReO_3, the lines at energies higher than 50 eV may have been connected to satellites, which can often be found in the spectra of the transition elements. The position of the doublets and the relative content of oxidized states varies for bimetallic systems. Fig. 3b shows the spectrum of Os 4f as they were situated in a close distance within the energy scale. The structure of the lines was slightly different than those in the metallic mono systems. Fig. 3c presents a comparison with the Os 4f and Re 4f bimetallic spectrum. Among the main doublets that could be ascribed to the metallic Re and Os, additional lines appeared, which could have been related to the formation of an alloy. However, there is no literature XPS data on such alloys and the appearance of low-binding energy doublets could have been an indication of an Re_xOs_y alloy. Moreover, the content of both elements that were derived from the photoemission line was close to 1:1, which can be expected when alloying occurs. However, the spectra of Re and Os were very rich in signals, which made completely identifying the structures by the direct fitting of the signals difficult.

A similar spectrum was obtained for the ReRu system (Re 4f) where the additional contribution from the Ru 4p line made the analysis complicated (Fig. 3d). Nevertheless, similar to the ReOs system, the

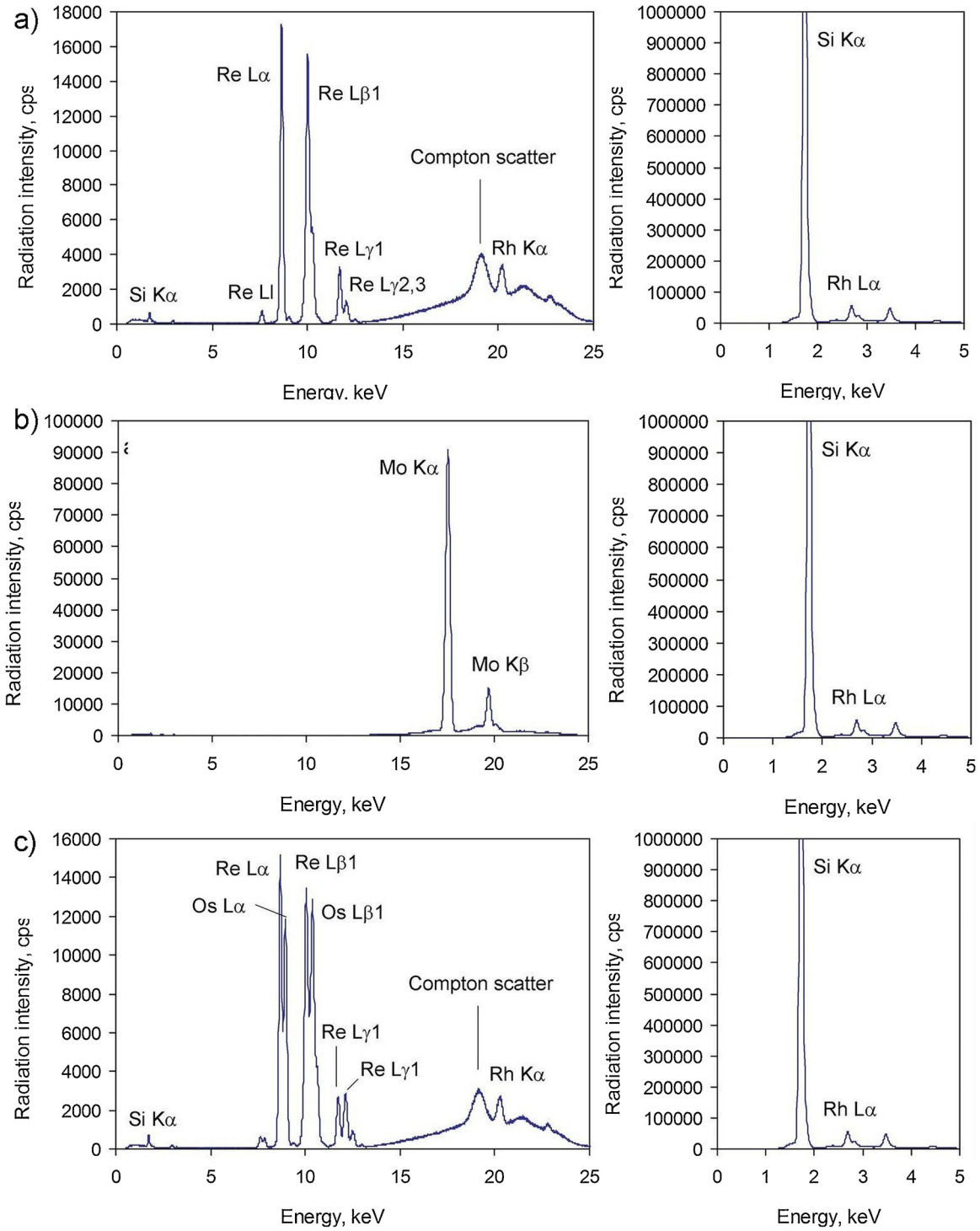

Fig. 1. Example EDXRF spectra of 1.0% Re/SiO_2 (A); 1.0% Mo/SiO_2 (B); 1.0% $ReOs(1:1)/SiO_2$ that were collected using an Rh target X-ray tube operating at 30 kV (determination of Re, Mo, Os) and 5 kV (determination of Si).

composition was also close to 1:1 and an additional doublet was observed in the Re 4f spectrum (Fig. 3d) while the Ru 3p (Fig. 3e) doublet had a metallic doublet in the energy close to the pure Ru.

For the ReMo and ReIr systems, the composition that was discovered from the XPS lines showed a surface enrichment in rhenium. This effect was even larger for the Re oxides. While Mo appeared on the surface mostly in an oxidized state, the Ir 4f line indicated that a metallic state was the dominant one.

In the Mo/SiO_2, Re/SiO_2 and $ReOs(1:1)/SiO_2$ systems, the metallic nanoparticles were distributed on the surface of SiO_2 the particles. They were arranged individually or in the form of conglomerates (Fig. 4a, c and e). The Re and Os had the same structure (space group $P6_3/mmc$), a similar atomic radius and their lattice parameter only differed slightly. Therefore, they formed solid solutions that had crystallite dimensions of about 5–15 nm (Fig. 4f). The chemical composition of these particles varied widely. The Re(Ru) particles were inhomogeneously distributed on the surface of SiO_2 (Fig. 4e).

Table 1
Results of EDXRF analysis of the SiO_2 supported catalysts.

Catalyst	Chemical element [wt%]				
	Re	Ru	Ir	Mo	Os
1.0% Re/SiO_2	0.95 ± 0.019	–	–	–	–
1.0% Ru/SiO_2	–	1.12 ± 0.023	–	–	–
1.0% Ir/SiO_2	–	–	0.98 ± 0.023	–	–
1.0% Mo/SiO_2	–	–	–	0.87 ± 0.055	–
1.0% Os/SiO_2	–	–	–		1.09 ± 0.041
1.0% $ReRu(1:1)/SiO_2$	0.55 ± 0.012	0.56 ± 0.010	–	–	–
1.0% $ReIr(1:1)/SiO_2$	0.53 ± 0.010	–	0.49 ± 0.016	–	–
1.5% $ReMo(2:1)/SiO_2$	1.07 ± 0.066	–	–	0.50 ± 0.029	–
1.0% $ReOs(1:1)/SiO_2$	0.84 ± 0.050	–	–	–	0.56 ± 0.031

3.2. Catalyst activity in the acetalization of polyols

The acetalization of glycerol, propylene glycol or ethylene glycol was catalyzed by the systems that were based on Re that had been doped with Os, Ir, Ru or Mo. The reacting polyol and acetone were prepared at a molar ratio of 1:10. The synthesis was run without an inert gas. Moreover, the synthesis did not demand the addition of a strong organic or inorganic acid or an additional solvent. Although an ambient temperature was sufficient, an optional increase to 55 °C at ambient pressure was found to be optimal for yielding the product in ca. one hour. Based on our previous experience with the application of catalytic methods for the synthesis of different products [2,10,22], we used sol-gel silica (< 4 μm) as the support for the nanoparticles. This permitted the correct wetting ability of the catalyst system as well as ensuring the uniform porosity and polydispersity of the nanoparticles that were placed on the silica. Additionally, a mild acidity of a carrier can enhance acetalization [22].

The results of the acetalization of ethylene glycol with acetone are summarized in Table 3. Of the five d-block metals (Re, Ru, Ir, Mo, Os) that were deposited on sol-gel silica, the highest catalytic activity was observed for Re (TON = 1242), for which we observed a 100% selectivity of 2,2-dimethyl-1,3-dioxolane (DMD) synthesis. In compare with the Re system in the monometallic Mo and Ru systems, we observed a change of selectivity to 2-(2-hydroxyethoxy)propan-2-ol (HEP) 0% vs. 15.4% vs. 58.8% respectively (Table 3, entries 1, 2, 4). We also observed a significantly higher conversion rate for Re (66.7%) and Mo (20.6%) than for Ru (6.4%). The other catalytic systems, e.g. Os and Ir were characterized by a low conversion rate (α = 2.7–4.5%) with 100% selectivity HEP was formed (Table 3, entries 3 and 5). The highest conversion rate and TON (68.4% and 1294 respectively) were obtained for the 1.0% $ReIr(1:1)/SiO_2$ system. Compared to 1.0% Mo/SiO_2, 1.5% $ReMo(2:1)/SiO_2$, increased the selectivity of the main product (84.6% vs. 93.3%). Bimetallic Re catalytic systems doped with Os, Ru were characterized by comparable values of the conversion rate (Table 3, entries 7, 8), but a significant increase in the selectivity of DMD synthesis in comparison with their monometallic counterparts were observed (Table 3, entries 3, 4 vs. 7, 8).

The same set of catalysts was also tested for the reaction of propylene glycol with acetone. The results are presented in Table 4. Among the monometallic catalysts, Re and Mo had a conversion rate of 77.8% and 33.8%, respectively. We observed a 100% selectivity of 2,2,4-trimethyl-1,3-dioxolane (TMD). The other monometallic catalysts, Os, Ru and Ir, had a very low conversion rate (about 2–2.6%), which was comparable to the metal carriers alone, while 2-(2-hydroxypropan-2-yloxy)propan-1-ol (HPP) was the preferred product in this case (Table 4, entries 3–5 vs. 10). Better conversion rates were observed for the bimetallic ReIr and ReRu catalysts (84.1% vs. 92%), especially, when compared with the 1.0% Re/SiO_2, ReOs and ReMo systems (Table 4, entry 1 vs. 6–9).

In the tested bimetallic systems, Re that had been doped with Os, Mo, Ir or Ru can interacted synergistically and induced both an increase or decrease of the reaction productivity. At the same time the transition products accompanied the expected final reaction products. Accordingly, the reaction selectively proceeds one of the possible ways but the reactants are not fully reacted. Accordingly, the conversion and TON seems to better explain the process. In general, every bimetallic system is more active in all three reactions with respect to monometallic systems. Some other effects may be due a formation of metal alloys. One of the conditions for the formation of a metallic alloy is crystallization in the same crystallographic system. Elements Re, Os and Ru crystallize in a hexagonal arrangement – hcp, Mo in body centered cubic (bcc) and Ir in cubic faced centered (fcc) system. The partial presence of alloyed metal structures was confirmed using the XPS technique (Fig. 3a–e) for the ReOs and ReRu catalysts, but not for the ReIr and ReMo systems. For example, higher conversion rates of propylene glycol – acetone system (Table 4, entry 6 and 8 vs. 1) were observed in the alloyed ReRu (α = 92%), vs. the unalloyed ReIr (α = 84.1%). Both of these compared advantageously to the Re catalyst (α = 77.8%). For the metals from groups VIII–XI the catalytic activity could be explained partly by the degree to which the d shell filled, which influences the strength of the adsorption of reagents and intermediates [56]. The electron properties that influence catalytic activity were linked to the ionization energy and the electronegativity of the elements (Table S8, Supplementary materials). Low values of the ionization energy combined with a low electronegativity (χ) are conducive for a reaction. For example, Re (760; 1260 kJ/mol (I, II), 1.9 (χ)) is much more reactive than Ir (880; 1600 kJ/mol (I, II), 2.2 (χ)). Another example is the much more active Mo (684.3, 1560 kJ/mol (I, II), 2.16 (χ)) than Ru (710.2, 1620 kJ/mol (I, II), 2.2 (χ)). The sizes of the nanoparticles that were determined using XRD (Table 2) in the bimetallic nanoparticles Re and the doped metals were much smaller, which may explain the higher activity of the catalyst systems that resulted [57]. This effect is particularly evident when comparing the degree of the conversion rate in the ReIr, ReRu systems with the Re catalyst (Table 4 entries 6 and 8 vs. 1) with the results in Table 2, e.g. for the unalloyed ReIr catalyst α = 84.1% (D_{Re} = 6.0 nm), while for the alloyed ReRu catalyst, α = 92% (D_{Re} = 6.0 nm) and for the monometallic Re catalyst, α = 77.8% (D_{Re} = 8–10.0 nm).

For the reaction of glycerol with acetone (Table 5), we observed a 100% conversion rate for the 1.0% Re/SiO_2 catalyst, which also provided a high selectivity (97.1%) towards the thermodynamically favored five-membered 2,2-dimethyl-1,3-dioxolane – DDM. The selectivity of the catalysts 1.0% Mo/SiO_2 and 1.0% Ru/SiO_2 (Table 5, entries 2 and 4) to a six-membered ring, i.e. 2,2-dimethyl-1,3-dioxan-5-ol (15.3% and 26.5%, respectively) was observed; however, with a significantly lower conversion rate (α = 68.4% and 15% respectively). Once again, we did not observe a significant increase in the catalytic activity of the monometallic Os and Ir catalysts compared to SiO_2. For all of the bimetallic systems, we observed a 100% conversion rate and a similar selectivity of the solketal synthesis – DDM oscillated around 86–91%. The highest TON value was observed in oscillating ReIr and ReOs system (TON = 1892 and 1882, respectively). The last factor that

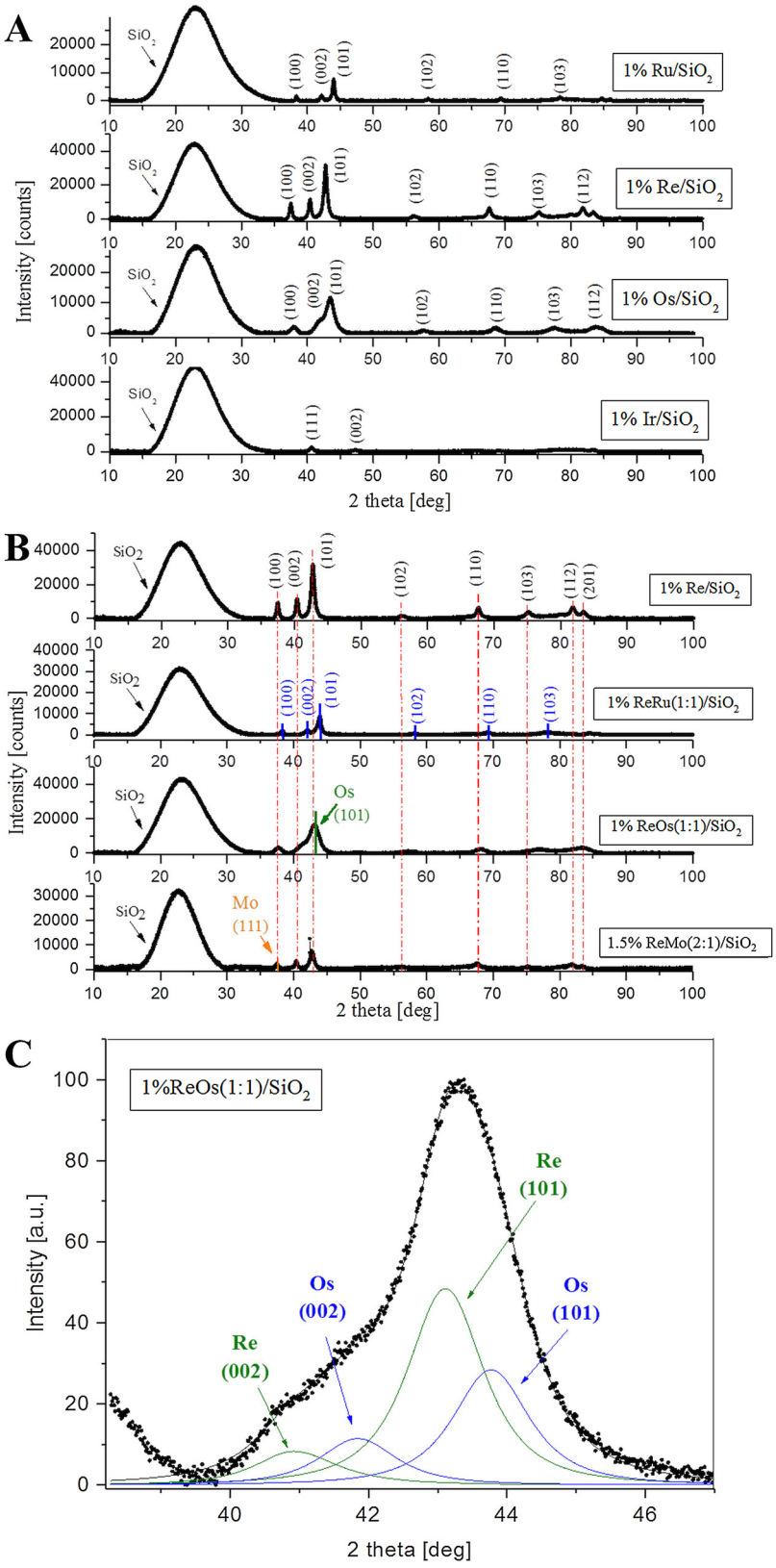

Fig. 2. (A) The X-ray diffraction patterns of the Re, Os, Ir and Ru silica-supported catalysts. The Miller indices for experimental peaks are marked. (B) The X-ray diffraction patterns of the 1.0% ReIr(1:1)/SiO_2, 1.0% ReRu(1:1)/SiO_2, 1.0% ReOs(1:1)/SiO_2 and 1.5% ReMo(2:1)/SiO_2 samples in the 20°–100° 2θ range. The Miller indices for experimental peaks of Re (black) and Ru (blue) are marked. For Os and Mo, only the most intensive diffraction lines are given. (C) Decomposition of the XRD pattern of 1.0% ReOs(1:1)/SiO_2 in a range of the 2θ angle from 38 to 47°. Experimental data (points), fitted data (full lines). In order to make the figure clearer, only the $K_{\alpha 1}$ lines are shown (For interpretation of the references to colour in this figure legend, the reader is referred to the web version of this article).

influences the conversion rate and selectivity of formed products of a polyol-acetone system is the type of starting substrate (Scheme 1). If the reagent is diol, the only acetalization product is a five-membered cyclic acetal or acyclic product. If the reagent is glycerol, it is also possible to form a six-membered ring. After some time, this is converted into a thermodynamically preferential five-membered solketal (DDM). For the glycerol-acetone system, we observed the complete conversion of alcohol due to the possibility to form several acetalization products – DDM, DDL and OPE. In the final stage of the reaction, DDL and OPE were transformed into solketal DDM. This is possible when DDL is not stable and affects the equilibrium, thus favoring the formation of a thermodynamically privileged product (DDM).

Table 2
XRD measurement results of the average size diameters for the selected Re NPs catalysts supported at SiO_2.

Catalyst	Lattice parameters [Å]	D[a] (nm) Re	D[a] (nm) Ru	D[a] (nm) Os	D[a] (nm) Mo	D[a] (nm) Ir
1.0% Re/SiO_2	for Re a = 2.771 (± 0.005) c = 4.462 (± 0.001)	8.0-10.0	–	–	–	–
1.0% Ru/SiO_2	for Ru a = 2.711 (± 0.004) c = 4.289 (± 0.003)	–	10.0-11.0	–	–	–
1.0% Os/SiO_2	for Os a = 2.738 (± 0.005) c = 4.326 (± 0.003)	–	–	3.0	–	–
1.0% Mo/SiO_2	N/D	–	–	–	N/D	–
1.0% Ir/SiO_2	for Ir a = 3.844 (± 0.009)	–	–	–	–	6.0
1.0% $ReRu(1:1)/SiO_2$	for Ru a = 2.715(± 0.002) c = 4.297(± 0.001)	6.0	6.0-7.0	–	–	–
1.0% $ReOs(1:1:)/SiO_2$	for Re a = 2.773(± 0.005) c = 4.465(± 0.006) for Os a = 2.730(± 0.004) c = 4.321(± 0.006)	4.0	–	3.0	–	–
1.5% $ReMo(2:1:)/SiO_2$	for Re a = 2.775(± 0.004) c = 4.466(± 0.007) for Mo a = 4.158(± 0.006)	7.0	–	–	6.0	–
1.0% $ReIr(1:1:)/SiO_2$	for Ir a = 3.835(± 0.007) for Re a = 2.771(± 0.005) c = 4.470(± 0.004)	6.0	–	–	–	5.0

N/D – not determined.
[a] Calculations for the (101) diffraction line of Re, Os, Ru and for the (111) peak in case of Ir and Mo.

A comparison of Re and Mo catalysts in all three reaction systems (Table 3, entries 1 and 2; Table 4, entries 1 and 2 vs. Table 5, entries 1 and 2) revealed a significant increase to other describe catalytic systems in the conversion rate and catalytic activity e.g. 1.0% Re/SiO_2 (TON = 1242 vs. 1449 vs. 1862) and 1.0% Mo/SiO_2 (TON = 198 vs. 324 vs. 656). There was moderate activity increase for 1.0% Ru/SiO_2 that yielded a TON of 65–152 (Table 3 entry 4 vs. Table 5 entry 3) and a lower for the Os and Ir monometallic systems where TON oscillated between 38–86 (Table 3 entries 3 and 5; Table 4, entries 3 and 5; Table 5, entries 3 and 5). Interestingly, for the bimetallic systems ReIr, ReOs, we observed only slightly higher or comparable TON values compared to 1.0% Re/SiO_2 (Table 3, entries 6–7, Table 4 entries 6–7, Table 5 entries 6–7). In turn, in the bimetallic systems in which Re had been doped with Ru and Mo, a significant decrease in catalytic activity was observed (Table 3, entries 8–9, Table 4 entries 8–9, Table 5 entries 8–9).

In additional experiments we checked the catalytic properties of 1.0% Re/SiO_2 in acetalization of polyols with others ketones (2-butanone and 3-pentanone). The results were collected in Table 6. In the reactions with diols and 2-butanone or 2-pentanone we did not observe any catalytic activity of the carrier (Table 6, entries 1, 3, 5, 7). In contrast the carrier activity in reaction with the same set of ketones with glycerol conversion rate was ca. 6.1% and mainly intermediate product were observed with 100% selectivity (Table 6, entries 9 and 11). The conversion rate for all three reactions with polyols decreases as follows: acetone, 2-butanone, 3-pentanone which agrees with the increasing of the steric hindrance for ketones (Tables 3–5 entries 1 vs. Table 6, entries 2, 4, 6, 8, 10, 12). The selectivity of the reaction of glycerol with 2-butanone or 3-propanone towards a formation of main acetal product is similar amounting to 94.6% vs. 88.9%. In turn, the selectivity towards intermediate product is almost two times lower in reaction with 2-butanone (Table 6, entries 10 vs. 12). We compared the results for the 1.0% Re/SiO_2 system with the results reported for the homogenous catalytic system [58]. Mononuclear or polynuclear copper complexes are well known and useful catalyst of the acetalization of alcohols. These catalysts are also efficient in chiral synthesis approaches [59,60]. For example, $[Cu^{I}_4Cu^{II}(mtpo)_4(H_2O)_2Cl_2]_n$ catalyzes acetalization of ethylene glycol with 2-butanone in toluene providing the conversion of 47% in 24 h at 90 °C [61]. However, the amount of this catalyst needed was 0.1 mol%. In contrast as low as 4.87×10^{-6} mol% of the heterogeneous catalyst reported in this publication, namely, 1.0% Re/SiO_2 in the same reaction provided the conversion rate of 63.8% in 1 h at 55 °C. Further, other advantages of reported heterogeneous catalysts are durability during storage, possibility of multiple use, ease of separation from the reaction mixture and their low costs of operation and regeneration.

The catalytic activity of 1.0% Re/SiO_2 compared to the literature data for the HZSM-5 and Amberlyst-36 catalysts [62–65] is presented in Table 7. The scale was enlarged ten times for the catalyst and 100 times for the reacting reagents. The new Re systems compared advantageously to all of the previously tested HZSM-5 or Amberlyst-36 systems, in which no more than a 5% conversion rate was achieved. For example, the acetalization of ethylene glycol to 2,2-dimethyl-1,3-dioxolane gave a 51% yield, whereas the yield of 2,2,4-trimethyl-1,3-dioxolane from propylene glycol was 74.4%. Additionally, the HZSM-5 and Amberlyst-36 required the use of strong organic or inorganic acids (H_2SO_4, p-toluenesulfonic acid), additional solvents (1,4-dioxane, tetrahydrofuran, cyclohexane, dichloromethane), a long synthesis time (3–24 h) and use of a Dean-Stark apparatus to remove the water from the reaction environment [30–41,66]. In addtion to the above-mention factors, an important innovation for nano-Re catalysts is a shorter synthesis time and an easy separation from the post-reaction mixture. Considering the advantages of the nano-Re catalyst, which is an ecological method for acetal separation, the possibility of the recovery of

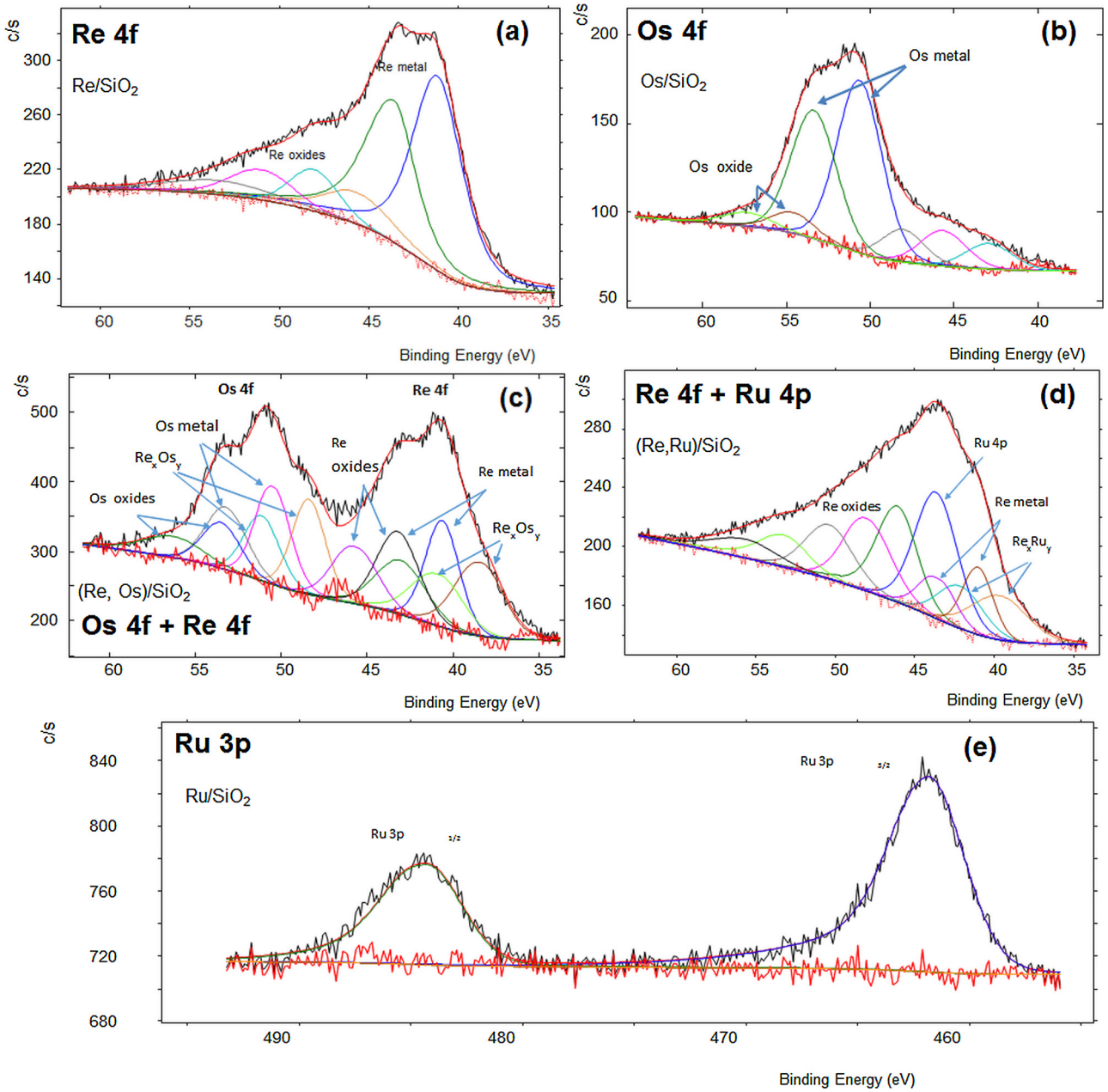

Fig. 3. The XPS spectra of the most prominent energy levels for the mono- and bimetallic Re nano-systems, a – Re 4f level with the result of fitting for the Re nanopowder, b – Os 4f line for the Os mono- system, c – Re 4f and Os 4f for the bimetallic system, d – Re 4f line for the ReRu system, e – Ru 3p doublet for the ReRu system.

substrates and the possibility to reuse the catalyst [22], this method is currently one of the most promising, competitive and economically profitable.

3.3. Cyclic acetals as potential additives to diesel oil

The thermophysical properties of pure cyclic acetals were studied in order to confirm their potential application as additives to diesel fuel. We examined the effect of temperature on the density (ρ), viscosity (ν), isentropic compressibility (κ_S) and isobaric thermal expansion (α_p) of DDM, TMD and DMD. We also examined two types of commercial petroleum diesel oil (labelled diesel[1] and diesel[2]) and mixtures of 1% vol. DDM + diesel[1] or + diesel[2] and mixtures of (0.5% vol. DDM and 0.5% vol. TMD) + diesel[1] or + diesel[2]. For this reason, the speed of sound was measured at temperatures ranging from 10 °C to 70 °C. The results are presented in Tables S9 and S10, Supplementary materials. The density was measured in a temperature range of 5 °C to 90 °C and these results are presented in Tables S9 and S10, Supplementary materials. The viscosity was measured for temperatures of 20 °C to 50 °C. The results were collected in Tables S9 and S10, Supplementary materials. The isentropic compressibility was calculated using the Laplace-Newton equation $\kappa_S = (\rho \cdot c^2)^{-1}$. The results are presented in Tables S9 and S10, Supplementary materials. The isobaric thermal expansion was calculated from the definition of $\alpha_p = -(1/\rho)(\partial\rho/\partial T)_p$ using second-order polynomial function for fitting the ρ (T) dependence. The results are presented in Tables S9 and S10, Supplementary materials. Important properties that can affect the suitability of any material such as diesel fuel are specified in the diesel standards (European Standard for diesel EN 590). The corresponding specifications for diesel[1], diesel[2], mixtures of 1% vol. DDM + diesel[1] or + diesel[2] and mixtures of (0.5% vol. DDM and 0.5% vol. TMD) + diesel[1] or + diesel[2] are presented in Table 8. Additionally, the biodiesel based on the fatty acid methyl esters

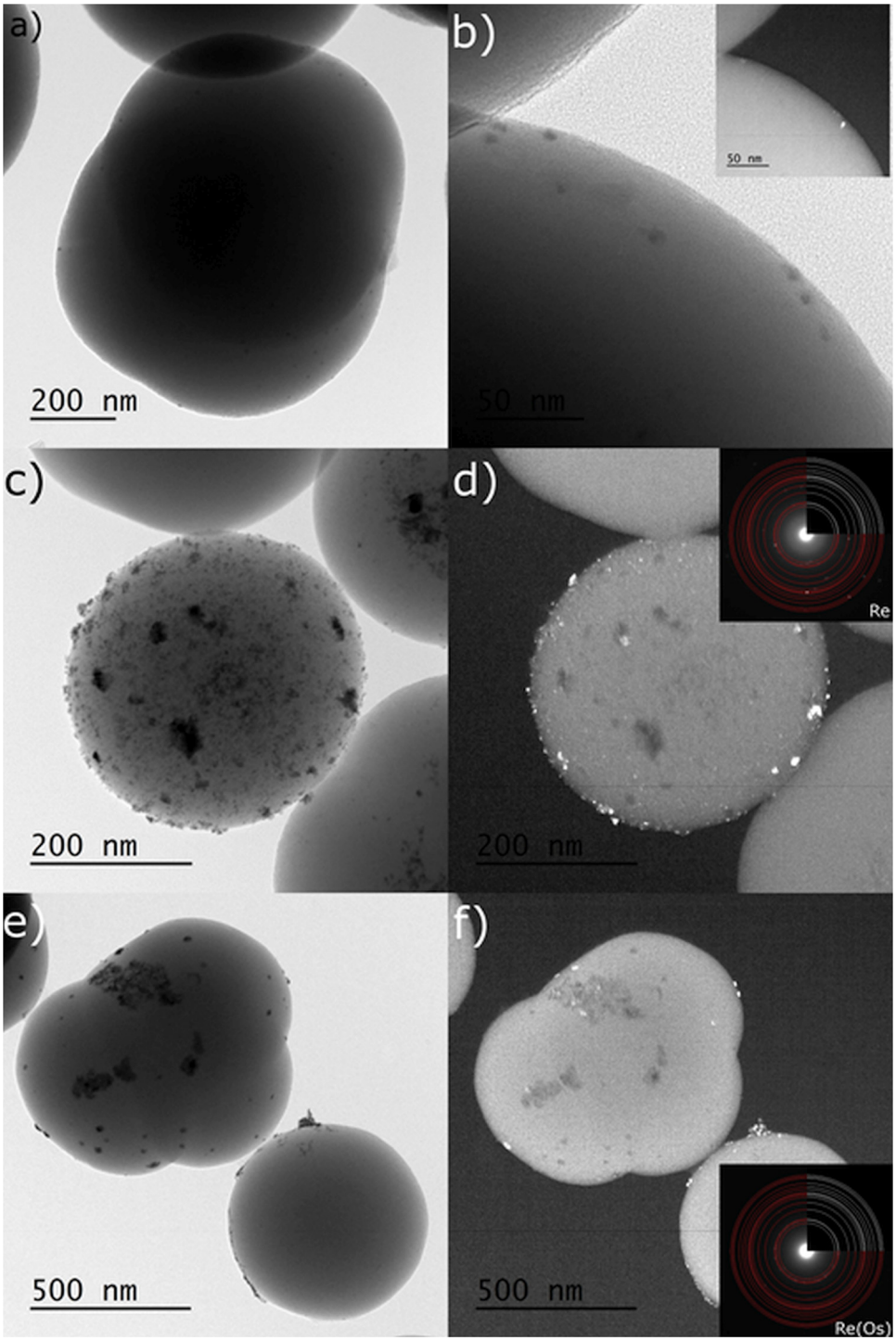

Fig. 4. Representative TEM images of the 1.0% Mo/SiO_2, 1.0% Re/SiO_2 and 1.0% ReOs(1:1)SiO_2 catalysts. a – nanoparticles of the Mo phase on the surface of SiO_2, b – magnification of the particles with a dark field insight, c, d – nanoparticles of the Re phase on the SiO_2 carrier and e, f – ReOs nanoparticles on the surface of the sol-gel silica.

of rapeseed oil [47,67] was selected for comparison. The diesel[1] and diesel[2] fulfilled norm EN 590 (Tables S6 and S7, Supplementary materials) and biodiesel fulfilled norm EN 14214 [47].

The density of pure DDM, TMD and DMD was higher than diesel[1] and diesel[2] (according to EN 590) or biodiesel (according to EN 14214). In order to illustrate this, the density of DDM, TMD and DMD was compared with diesel[1], diesel[2] and biodiesel (Fig. 5A). DDM had the highest density values. The density of DDM was about 17% higher than the density of biodiesel and about 22% higher than petroleum diesel oils (diesel[1] and diesel[2]) over the entire temperature range. The differences between density of DMD and TMD and the density of petroleum petroleum diesel oils (diesel[1] and diesel[2]) and biodiesel decreased with increasing temperature. The density of DMD was about 7% higher than biodiesel and about 13% higher than petroleum diesel oils (diesel[1] and diesel[2]) at 15 °C. The density of TMD was about 8% higher than petroleum diesel oils (diesel[1] and diesel[2]) at 15 °C. The density of TMD was the closest to biodiesel and with an increasing temperature, the differences decreased from 3% at 5 °C to 0.4% at 70 °C. The addition of

Table 3
Catalytic performance of mono- and bimetallic Re, Mo, Os, Ru, Ir NPs systems supported on SiO_2 in ethylene glycol acetalization with acetone[a].

	Catalyst	α[b] [%]	TON[c]	Selectivity[d] [%]		Yield DMD [%]
				DMD	HEP	
1	1.0% Re/SiO_2	66.7	1242	100	0	66.7
2	1.0% Mo/SiO_2	20.6	198	84.6	15.4	17.4
3	1.0% Os/SiO_2	4.5	86	0	100	0
4	1.0% Ru/SiO_2	6.4	65	41.2	58.8	2.6
5	1.0% Ir/SiO_2	2.7	52	0	100	0
6	1.0% ReIr(1:1)/SiO_2	68.4	1294	100	0	68.4
7	1.0% ReOs(1:1)/SiO_2	62.3	1172	100	0	62.3
8	1.0% ReRu(1:1)/SiO_2	65.6	860	100	0	65.6
9	1.5% ReMo(2:1)/SiO_2	61.7	583	93.3	6.7	57.6
10	SiO_2	2	0	0	100	0

[a] 1.24 mol/L of ethylene glycol in the reaction mixture (ethylene glycol/acetone molar ratio 1:10), 50 mg of catalyst (1.3–2.7 μmol Re), ultrasounds 10 min, 55 °C, 1 h, 200 rmp.
[b] α – system conversion rate.
[c] Turnover number (TON) based on the total content of metal NPs in the material calculated based on Eq. (4).
[d] DMD – 2,2-dimethyl-1,3-dioxolane, HEP – 2-(2-hydroxyethoxy)propan-2-ol.

Table 4
Catalytic performance of mono- and bimetallic Re, Mo, Os, Ru, Ir NPs systems supported on SiO_2 in propylene glycol acetalization with acetone[a].

	Catalyst	α[b] [%]	TON[c]	Selectivity[d] [%]		Yield TMD [%]
				TMD	HPP	
1	1.0% Re/SiO_2	77.8	1449	100	0	77.8
2	1.0% Mo/SiO_2	33.8	324	100	0	33.8
3	1.0% Os/SiO_2	2.3	44	0	100	2.3
4	1.0% Ru/SiO_2	2.6	26	0	100	2.6
5	1.0% Ir/SiO_2	2	38	0	100	2
6	1.0% ReIr(1:1)/SiO_2	84.1	1591	100	0	84.1
7	1.0% ReOs(1:1)/SiO_2	76.4	1438	100	0	76.4
8	1.0% ReRu(1:1)/SiO_2	92	1205	100	0	92
9	1.5% ReMo(2:1)/SiO_2	78.2	739	100	0	78.2
10	SiO_2	1.9	0	0	100	0

[a] 1.21 mol/L of propylene glycol in the reaction mixture (propylene glycol/acetone molar ratio 1:10), 50 mg of catalyst (1.3–2.7 μmol Re), ultrasounds 10 min, 55 °C, 1 h, 200 rmp.
[b] α – system conversion rate.
[c] Turnover number (TON) based on the total content of metal NPs in the material calculated based on Eq. (4).
[d] TMD – 2,2,4-trimethyl-1,3-dioxolane, HPP – 2-(2-hydroxypropan-2-yloxy) propan-1-ol.

1% vol. DDM or a mixture of 0.5% vol. DDM with 0.5% vol. TMD into the petroleum diesel oils (diesel[1] or diesel[2]) did not change their density significantly (see Tables S2–S5, Supplementary materials). The maximum difference equaled 0.26%. This is crucial because the density affects the conversion of the volume flow rate into the mass low rate and the total amount of fuel that is injected into a cylinder. A precisely adjusted amount of fuel is necessary to provide the proper combustion. The combustion process is strongly affected by density. Therefore, the adaptation of injection systems to biofuels requires an accurate knowledge of the effect of temperature and pressure on their volumetric properties. The density of DDM, TMD and DMD decreased almost linearly with an increasing temperature, but the slope of the isobar of DDM was similar to diesel[1], diesel[2] and biodiesel. It is, however, clear that compared to TMD and DMD, it is different.

Isobaric thermal expansion characterizes how temperature affects density. The isobaric thermal expansion values of DMD and TMD were

Table 5
Catalytic performance of mono- and bimetallic Re, Mo, Os, Ru, Ir NPs systems supported on SiO_2 in glycerol acetalization with acetone[a].

	Catalyst	α[b] [%]	TON[c]	Selectivity[d] [%]			Yield DDM [%]
				DDM	DDL	OPE	
1	1.0% Re/SiO_2	100	1862	97.1	2.0	0.9	97.1
2	1.0% Mo/SiO_2	68.4	656	77.6	15.3	7.1	53.1
3	1.0% Os/SiO_2	3.8	72	0	0	100	0
4	1.0% Ru/SiO_2	15	152	54.8	26.5	18.7	8.2
5	1.0% Ir/SiO_2	3.6	69	0	0	100	0
6	1.0% ReIr(1:1)/SiO_2	100	1892	87.8	5.3	6.9	87.8
7	1.0% ReOs(1:1)/SiO_2	100	1882	91.4	5.5	3.1	91.4
8	1.0% ReRu(1:1)/SiO_2	100	1310	86.6	8.9	4.5	86.6
9	1.5% ReMo(2:1)/SiO_2	100	945	88.9	5.4	5.7	88.9
10	SiO_2	3.7	0	0	0	100	0

[a] 1.23 mol/L of glycerol in the reaction mixture (glycerol / acetone molar ratio 1:10), 50 mg of catalyst (1.3–2.7 μmol Re), ultrasounds 10 min, 55 °C, 1 h, 200 rmp.
[b] α – system conversion rate.
[c] Turnover number (TON) based on the total content of metal NPs in the material calculated based on Eq. (4).
[d] DDM – (2,2-dimethyl-1,3-dioxolan-4-yl)methanol – (solketal); DDL – 2,2-dimethyl-1,3-dioxane-5-ol; OPE – 3-(2-oxidanylpropan-2-yloxy)propane-1,2-diol.

almost equal to each other and were higher than DDM, petroleum diesel oils (diesel[1] and diesel[2]) and biodiesel (Fig. 5B). Significantly lower values of isobaric thermal expansion characterized DDM, petroleum diesel oils (diesel[1] and diesel[2]) and biodiesel. Moreover, the effect of temperature on their isobaric thermal expansion was less pronounced than in case of DMD and TMD. The maximum difference was observed between DMD and biodiesel (42% at 5 °C and 58% at 70 °C). The addition of 1% vol. DDM or a mixture of 0.5% vol. DDM with 0.5% vol. TMD into the petroleum diesel oils (diesel[1] or diesel[2]) affected the changes of the isobaric thermal expansion values of the petroleum diesel oils only slightly so that they can be omitted. The maximum difference equaled 0.5%.

Isentropic compressibility characterizes how pressure affects density. Depending on the operating modes of an engine, the injector opening position can be influenced by the isentropic compressibility and the speed of sound in fuels [68]. The compressibility changes that are associated with differences in the chemical structure between DDM, DMD, TMD and petroleum-based fuel can change the engine injection timing. Since the compressibility determines the spray characteristics upon injection, it is closely related to the content of greenhouse gases in exhausts.

The isentropic compressibility of all of the investigated systems increased non-linearly with an increasing temperature. Moreover, the differences between the isentropic compressibility values also increased with an increasing temperature (Fig. 5C). TMD was the most compressible and the effect of temperature on its isentropic compressibility was higher than all of the investigated liquids (Fig. 5C). DDM had the lowest compressibility. The addition of 1% vol. DDM into the petroleum diesel oils (diesel[1] and diesel[2]) did not change their compressibility. The maximum difference did not exceed 0.1%. As was the case with density and isobaric thermal expansion, the addition of the mixture of 0.5% vol. DDM with 0.5% vol. TMD into the petroleum diesel oils (diesel[1] and diesel[2]) affected the changes of their isentropic compressibility only slightly. The maximum difference equaled 0.4%.

Combustion is initiated through the atomization of fuel. The use of a viscous fuel leads to a poor atomization, which is responsible for premature injector coking and poor fuel combustion. A high viscosity leads

Table 6
Comparison of polyols acetalization in reaction with different ketones for support and Re NPs supported at silica.

	Reagents[a]		Carrier/catalyst	α[b] [%]	TON[c]	Selectivity[c] [%]		Yield [%]	
	Alcohol	Ketone				CA	OS	CA	OS
1	Ethylene glycol	2-butanone	SiO_2	0	0	0^{I}	0	0	0
2			1.0% Re/SiO_2	63.8	1188	97.8^{I}	2.2	62.4	1.4
3		3-pentanone	SiO_2	0	0	0^{II}	0	0	0
4			1.0% Re/SiO_2	39.8	741	100^{II}	0	39.8	0
5	Propylene glycol	2-butanone	SiO_2	0	0	0^{III}	0	0	0
6			1.0% Re/SiO_2	85.8	1598	99.2^{III}	0.8	85.1	0.7
7		3-pentanone	SiO_2	0	0	0^{IV}	0	0	0
8			1.0% Re/SiO_2	15.4	287	100^{IV}	0	15.4	0
9	Glycerol	2-butanone	SiO_2	6.1	0	0^{V}	100	0	6.1
10			1.0% Re/SiO_2[d]	92.6	1724	94.6^{V}	5.4	87.6	5.0
11		3-pentanone	SiO_2	5.6	0	0^{VI}	100	0	5.6
12			1.0% Re/SiO_2	67.4	1255	88.9^{VI}	11.1	59.9	7.5

[a] 1.24 mol/L of ethylene glycol or 1.21 mol/L of propylene glycol or 1.23 mol/L of glycerol in the reaction mixture (polyol / ketone molar ratio 1:10), 50 mg of carrier / catalyst (2.7 μmol Re), ultrasounds 10 min, 55 °C, 1 h, 200 rmp.
[b] α – conversion rate.
[c] CA – main cyclic acetal product, (I - 2-ethyl-2-methyl-1,3-dioxolane; II - 2,2-diethyl-1,3-dioxolane; III - 2-ethyl-2,4-dimethyl-1,3-dioxolane; IV - 2,2-diethyl-4-methyl-1,3-dioxolane; V – (2-ethyl-2-methyl-1,3-dioxolan-4-yl)methanol; VI – (2,2-diethyl-1,3-dioxolan-4-yl)methanol), OS – other intermediate products.
[d] Reported previously in Table 5 [22].

Table 7
Catalytic activity of 1.0% Re/SiO_2 compared to the literature data.

	Reagents[a]	Catalyst	α[b] [%]	Selectivity[c] [%]		Yield [%]	
				CA	OS	CA	OS
1	Acetone	1.0% Re/SiO_2	51	100	0	51	0
	Ethylene glycol	HZSM-5	1.4	0	100	0	1.4
		Amberlyst-36	2	0	100	0	2
2	Acetone	1.0% Re/SiO_2	74.4	100	0	74.4	0
	Propylene glycol	HZSM-5	1.5	0	100	0	1.5
		Amberlyst-36	1.8	0	100	0	1.8
3	Acetone	1.0% Re/SiO_2[d]	100	96.5	3.5	96.5	3.5
	Glycerol	HZSM-5	0.5	0	100	0	0.5
		Amberlyst-36	4.5	42.5	57.5	1.9	2.6

[a] 1.24 mol/L of ethylene glycol or 1.21 mol/L of propylene glycol or 1.23 mol/L of glycerol in the reaction mixture (polyol / acetone molar ratio 1:10), 500 mg of catalyst (26.85 μmol Re), ultrasounds 10 min, 55 °C, 1 h, 200 rmp.
[b] α – conversion rate.
[c] CA – cyclic acetal (I – 2,2-dimethyl-1,3-dioxolane, II – 2,2,4-trimethyl-1,3-dioxolane, III – (2,2-dimethyl-1,3-dioxolan-4-yl)methanol – solketal), OS – other intermediate products.
[d] Reported previously in Table 6 [22].

to operational problems in a diesel engine, e.g. increased engine deposits. Since viscosity increases with a decreasing temperature, handling fuel at lower temperatures is facilitated by a lower viscosity. In the form of kinematic viscosity, this property is specified in the biodiesel standards (EN14214) with minimum value equal 3.5 $mm^2 s^{-1}$ and maximum value equal 5.0 $mm^2 s^{-1}$ at 40 °C. The minimum value for kinematic viscosity in the European standard exceeds that of most petrodiesel fuels which does not appear to be technically justified. In turn, in the United States, the biodiesel kinematic viscosity standard (ASTMD6751) can vary from 1.9 $mm^2 s^{-1}$ to 6.0 $mm^2 s^{-1}$ at 40 °C. Among all of the components that were studied, the highest kinematic viscosities were recorded for DDM. The effect of temperature on kinematic viscosity of DDM is also significant. Thus, the viscosity of DDM equaled 5.12 $mm^2 s^{-1}$ at 40 °C, which slightly exceeds the European, but fulfills the US biodiesel standard (ASTMD671). TDM and DMD had a considerably lower viscosity than DDM and the petroleum diesel oils (diesel[1] and diesel[2]) (Fig. 5D). The viscosity of TDM and DMD equaled 0.62 $mm^2 s^{-1}$ and 0.61 $mm^2 s^{-1}$ at 40 °C, respectively, which does not fulfill either the diesel nor biodiesel standards. However, the addition of 1% vol. of DDM into the petroleum diesel oils (diesel[1] or diesel[2]) did not change the viscosity significantly, i.e. the viscosity decreased in the range of 0.4 to 1.3%. Over the entire temperature range, the viscosity value for the blend of the petroleum diesel oils (diesel[1] or diesel[2]) with 0.5% vol. of DDM and 0.5% vol. TMD was in about 2% lower than the viscosity for the petroleum diesel oils (diesel[1] or diesel[2]). Therefore, cyclic acetals can be used to improve the viscosity of fuels. This allowed the optimal viscosity and the advantageous viscosity temperature dependence to be maintained.

Table 8
The results of the basic physico-chemical tests of DDM, TMD, DMD, diesel[1], diesel[2] and their mixtures.

Tested parameter/Unit/ Temperature	Diesel[1]	Diesel[2]	DMD[a]	TMD[b]	DDM[c]	Diesel[1] [d] + 1.0%vol. DDM : TMD (1:1)	Diesel[1] [d] + 1.0% vol. DDM	Diesel[2] [e] + 1.0%vol. DDM : TMD (1:1)	Diesel[2] [e] + 1.0% vol. DDM
ν /$mm^2 s^{-1}$/40 °C	2.87	2.77	0.61	0.62	5.12	2.81	2.85	2.73	2.75
ρ /kg m^{-3}/15 °C	832.66	833.86	950.31	907.31	1071.44	834.01	834.72	835.10	836.05
Water content/ppm	60.7	60.2	3500	700	900	70.6	77.0	65.0	72.2
$\kappa_S \cdot 10^{10}$/Pa^{-1}/15 °C	6.233	6.232	6.997	8.153	4.764	6.246	6.235	6.243	6.229
$\alpha_p \cdot 10^4$ /$°C^{-1}$/15 °C	8.367	8.383	11.791	11.776	8.266	8.398	8.401	8.417	8.427
Cetane number/-	52.7	55.3	–	–	–	52.5	51.5	56.5	52.7

[a] DMD – 2,2-dimethyl-1,3-dioxolane – see structure of cyclic acetal at Scheme 1.
[b] TMD – 2,2,4-trimethyl-1,3-dioxolane – see structure of cyclic acetal at Scheme 1.
[c] DDM – (2,2-dimethyl-1,3-dioxolan-4-yl)methanol – (solketal) – see structure of cyclic acetal at Scheme 1.
[d] See Table S6 in Supplementary materials.
[e] See Table S7 in Supplementary materials.

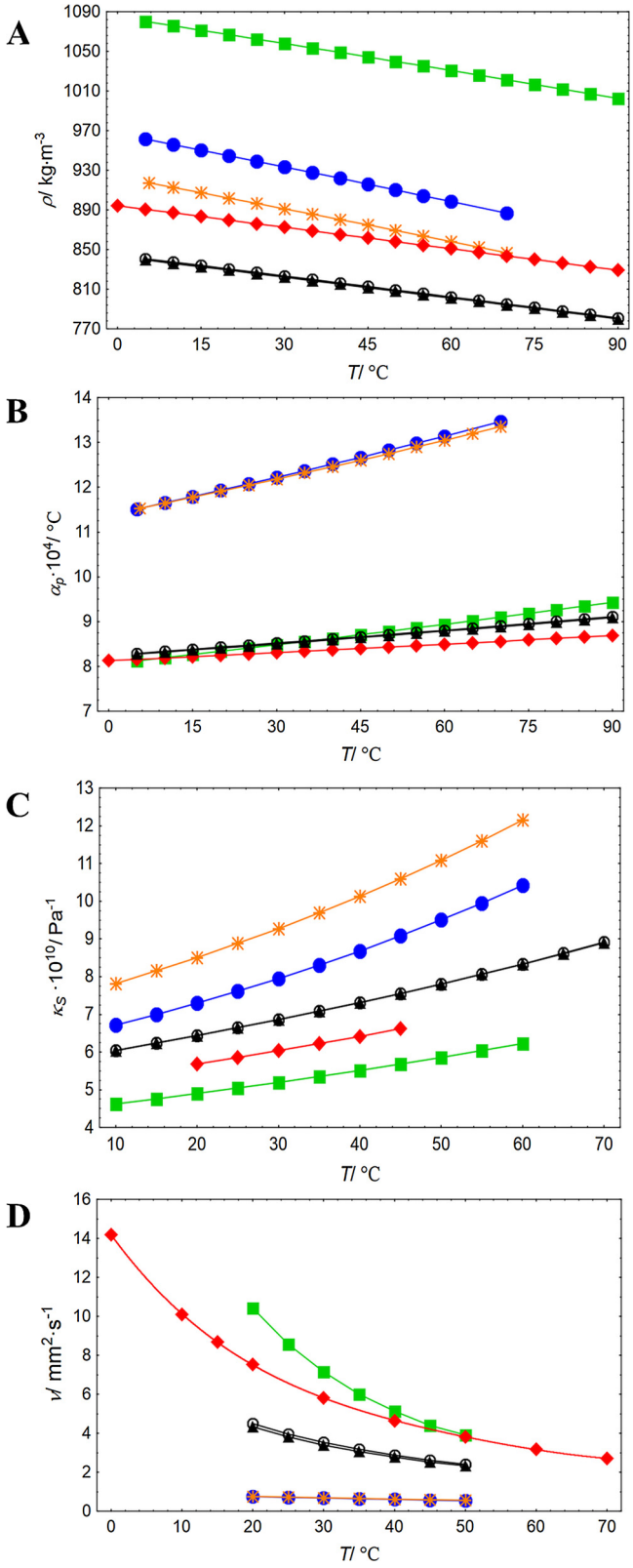

Fig. 5. Temperature dependencies of (A) density – ρ, (B) isobaric thermal expansion – α_p, (C) isentropic compressibility – κ_S (D) kinematic viscosity – ν of: ■ DDM; ● DMD; ✳ TMD; ○ diesel oil [1]; ▲ diesel oil [2]; ◆ biodiesel [47,67].

The cetane number is a dimensionless descriptor that is related to the ignition delay time a fuel experiences upon injection into the combustion chamber of a diesel engine. The higher the cetane number, the shorter the ignition delay time and vice versa. Increasing the CN to a certain level (around 60) has been connected with decreasing NOx exhaust emissions [69]. The CN is included in diesel and biodiesel standards with a prescribed minimum value of 51 according to EN 590 and EN 14214 and a minimum value of 47 according to ASTMD671. The CN of the blend of petroleum diesel[2] oil with 0.5% vol. of DDM and 0.5% vol. TMD increased about 2.2% compared to the petroleum diesel[2] oil (Table 8). The CN of the other investigated mixtures slightly decreased (about 2%) compared to the petroleum diesel oil. To summarize, all of the studied properties of cyclic acetals and their mixtures show that these products can be used as additives to improve fuel properties, particularly the cetane number and viscosity. In particular, the results obtained for the mixture of petroleum diesel[2] oil with 0.5% vol. of DDM and 0.5% vol. TMD are especially attractive, thus making it the best biofuel additive candidate.

4. Conclusions

In conclusion, we have reported here that the Re/SiO_2 catalyst can be a suitable low-cost catalyst for processing polyols into acetals with a high conversion rate and a selectivity of up to 100% in mild conditions. The byproducts of acetalization, if formed, are noncyclic products that can easily recycled to yield cyclic acetals.

In a complex investigation, we broadly tested the blending potential of the acetals that were formed by measuring the density, viscosity, isentropic compressibility, isobaric thermal expansion and other parameters of both the crude additives and the blends that were prepared with petroleum diesel oil. The results indicate that the investigated acetals can generally be used for blending with petroleum diesel oil in order to obtain the valuable biofuels that are in great demand in the contemporary transportation industry due to regulatory restrictions that have been introduced in order to protect the environment.

Acknowledgments

Marzena Dzida, Edward Zorębski, and Małgorzata Musiał are profoundly indebted to Anton Paar Poland for sharing the DSA 5000M Density and Sound Velocity Meter. The research was co-financed by The National Centre for Research and Development (NCRD) under grant TANGO1/266384/NCBR/2015.

Appendix A. Supplementary data

Supplementary material related to this article can be found, in the online version, at doi:https://doi.org/10.1016/j.apcatb.2018.07.071.

References

[1] Pagliaro Mario, Rossi Michele, The future of glycerol: new uses of a versatile raw material, RSC Green Chemistry Book Series, Cambridge, 2008, pp. 1–134 Ch1-8.
[2] M. Kapkowski, T. Siudyga, R. Sitko, J. Lelątko, J. Szade, K. Balin, J. Klimontko, P. Bartczak, J. Polanski, PLoS One 10 (11) (2015) 1–15, https://doi.org/10.1371/journal.pone.0142668 e0142668.
[3] M. Massa, A. Andersson, E. Finocchio, G. Busca, J. Catal. 307 (2013) 170–184.
[4] F.F. Sousa, A.C. Oliveira, J.M. Filho, G.S. Pinheiro, M. Giotto, N.A. Barros, Chem. Eng. J. 228 (2013) 442–448.
[5] A. Alhanash, E.F. Kozhevnikova, I.V. Kozhevnikov, Appl. Catal. A: Gen. 378 (2010) 11–18.
[6] J. Deleplanque, J.L. Dubois, J.F. Devaux, W. Ueda, Catal. Today 157 (2010) 351–358.
[7] B.M. Bell, J.R. Briggs, R.M. Campbell, S.M. Chambers, P.D. Gaarenstroom, J.G. Hippler, B.D. Hook, K. Kearns, J.M. Kenney, W.J. Kruper, D.J. Schreck, C.N. Theriault, C.P. Wolfe, Process Clean Soil Air Water 36 (2008) 657–661.
[8] E. Santacesaria, R. Tesser, M. Di Serio, L. Casale, D. Verde, Ind. Eng. Chem. Res. 49 (2010) 964–970.
[9] R. Tesser, E. Santacesaria, M. Di Serio, G. Di Nuzzi, V. Fiandra, Ind. Eng. Chem. Res. 46 (2007) 6456–6465.
[10] M. Kapkowski, P. Bartczak, M. Korzec, R. Sitko, J. Szade, K. Balin, J. Lelątko, J. Polanski, J. Catal. 319 (2014) 110–118.
[11] S. Carrettin, P. McMorn, P. Johnston, K. Griffin, G.J. Hutchings, Chem. Commun. 7 (2002) 696–697.
[12] S. Carrettin, P. McMorn, P. Johnston, K. Griffin, C.J. Kiely, G.J. Hutchings, Phys.

Chem. Chem. Phys. 5 (2003) 1329–10139.
[13] B. Katryniok, H. Kimura, E. Skrzyńska, J.S. Girardon, P. Fongarland, M. Capron, R. Ducoulombier, N. Mimura, S. Paul, F. Dumeignil, Green Chem. 13 (2011) 1960–1979.
[14] R.D. Cortright, R.R. Davda, J.A. Dumesic, Nature 418 (2002) 964–967.
[15] J.N. Chheda, G.W. Huber, J.A. Dumesic, Angew. Chem. Int. Ed. 46 (2007) 7164–7183.
[16] G.W. Huber, J.W. Shabaker, J.A. Dumesic, Science 300 (2003) 2075–2077.
[17] I. Furikado, T. Miyazawa, S. Koso, A. Shimao, K. Kunimoria, K. Tomishige, Green Chem. 9 (2007) 582–588.
[18] T. Miyazawa, Y. Kusunoki, K. Kunimori, K. Tomishige, J. Catal. 240 (2006) 213–221.
[19] J.A. Melero, R. Grieken, G. Morales, M. Paniagua, Energy Fuels 21 (2007) 1782–1791.
[20] C. Márquez-Alvarez, E. Sastre, J. Pérez-Pariente, Top. Catal. 27 (2004) 105–177.
[21] A.M. Ruppert, J.D. Meeldijk, B.W. Kuipers, B.H. Erné, B.M. Weckhuysen, Chem. Eur. J. 14 (2008) 2016–2024.
[22] M. Kapkowski, W. Ambrożkiewicz, T. Siudyga, R. Sitko, J. Szade, J. Klimontko, K. Balin, J. Lelątko, J. Polanski, Appl. Catal. B 202 (2017) 335–345.
[23] J.E. Vancauwenberge, P.J. Slininger, R.J. Bothast, Appl. Environ. Microbiol. 56 (1990) 329–332.
[24] F. Barbirato, P. Soucaille, C. Camarasa, A. Bories, Biotechnol. Bioeng. 58 (1998) 303–305.
[25] S. Vollenweider, C. Lacrox, Appl. Microbiol. Biotechnol. 64 (2004) 16–27.
[26] A.R. Trifoi, P.Ş. Agachi, T. Pap, Renew. Sustain. Energy Rev. 62 (2016) 804–814.
[27] F. Bär, H. Hopf, M. Knorr, O. Schröder, J. Krahl, Fuel 180 (2016) 278–283.
[28] I. Agirre, M.B. Güemez, A. Ugarte, J. Requies, V.L. Barrio, J.F. Cambra, P.L. Arias, Fuel Process. Technol. 116 (2013) 182–188.
[29] M.S. Khayoon, A. Abbas, B.H. Hameed, S. Triwahyono, A.A. Jalil, A.T. Harris, A.I. Minett, Catal. Lett. 144 (2014) 1009–1015.
[30] B. Mallesham, P. Sudarsanam, B.M. Reddy, Catal. Sci. Technol. 4 (2014) 803–813.
[31] B. Mallesham, P. Sudarsanam, G. Raju, B.M. Reddy, Green Chem. 15 (2013) 478–489.
[32] M.J. Climent, A. Corma, S. Iborra, Green Chem. 16 (2014) 516–547.
[33] D.Y. He, Z.J. Li, Z.J. Li, Y.Q. Liu, D.X.M.S. Qiu, Synth. Commun. 22 (1992) 2653–2658.
[34] C. Fan, C. Xu, C. Liu, Z. Huang, J. Liu, Z. Ye, Heterocycles 85 (2012) 2977–2986.
[35] C. Gonzalez-Arellano, S.R. Luque, Catal. Sci. Technol. 4 (2014) 4242–4249.
[36] Z.P. Han, Y. Li, Inorg. Chem. Commun. 22 (2012) 73–76.
[37] R. Rodrigues, M. Gonçalves, D. Mandelli, P.P. Pescarmona, W.A. Carvalho, Catal. Sci. Technol. 4 (2014) 2293–2301.
[38] C. Crotti, E. Farnetti, N. Guidolin, Green Chem. 12 (2010) 2225–2231.
[39] L. Shao, Y. Du, G. Xing, W. Lv, X. Liang, C. Qi, Monatsh. Chem. 143 (2012) 1199–1203.
[40] B. Wang, Y. Shen, J. Sun, F. Xua, Runcang Sun, RSC Adv. 4 (2014) 18917–18923.
[41] J.C. Meslard, F. Subira, J.P. Vairon, A. Guy, R. Garreau, Bull. Soc. Chim. Fr. 1 (1985) 84–89.
[42] R.H. Walsh, WO Pat., 1988005071 (1986).
[43] R. Jens, R. Rakoczy, R. Fischer, F. Rößner, A. Philipp, DE Pat., 102008015756 (2008).
[44] S.D. Varfolomeev, G.A. Nikiforov, V.B. Volieva, G.G. Makarov, L.I. Trusov, WO Pat., 2009145674 (2009).
[45] P.J. Mcdougall, WO Pat., 2012071154 (2011).
[46] S. Nicolas, F. Grigoletto, S. Martins, WO Pat., 2017006142 (2015).
[47] M. Dzida, P. Prusakiewicz, Fuel 87 (2008) 1941–1948.
[48] M. Dzida, S. Jężak, J. Sumara, M. Żarska, P. Góralski, Fuel 111 (2013) 165–171.
[49] M. Dzida, S. Jężak, J. Sumara, M. Żarska, P. Góralski, J. Chem. Eng. Data 58 (2013) 1955–1962.
[50] M. Żarska, K. Bartoszek, M. Dzida, Fuel 125 (2014) 144–151.
[51] S. Jężak, M. Dzida, M. Zorębski, Fuel 184 (2016) 334–343.
[52] K.S. Rao, K. El-Hami, T. Kodaki, K. Matsushige, K. Makino, J. Colloid Interface Sci. 289 (2005) 125–131.
[53] H. Okudera, A. Hozumi, Thin Solid Films 434 (2003) 62–68.
[54] J. Skowronek, M. Geppert-Rybczyńska, J. Jacquemin, P. Goodrich, J.V. Alvarez, M. Chorążewski, S. Jężak, E. Zorębski, M. Zorębski, M. Żarska, W. Kaca, P. Berdyczko, M. Dzida, J. Solut. Chem. 44 (2015) 824–837.
[55] I. Aruna, B.R. Mehta, L.K. Malhotra, S.M. Shivaprasad, J. Appl. Phys. 104 (2008) 064308-5.
[56] W.D. Wei, B.C. Sweeny, J. Qiu, J.S. DuChene, Metallic nanostructures forcatalytic applications, in: Yujie Xiong, Xianmao Lu (Eds.), Metallic Nanostructures: From Controlled Synthesis to Applications, Springer Inc., New York, 2015, pp. 243–271.
[57] L. Ilieva, P. Petrova, T. Tabakova, R. Zanella, M.V. Abrashev, J.W. Sobczak, W. Lisowski, Z. Kaszkur, D. Andreeva, Catal. Today 187 (2012) 30–38.
[58] S. Krompiec, M. Penkala, K. Szczubiałka, E. Kowalska, Coord. Chem. Rev. 256 (2012) 2057–2095.
[59] Q.J. Liu, L. Wang, Q.K. Kang, X.P. Zhang, Y. Tang, Angew. Chem. Int. Ed. 55 (2016) 9220–9223.
[60] A.F. Garrido-Castro, M.C. Maestro, J. Alemán, Tetrahedron Lett. 59 (2018) 1286–1294.
[61] Z.P. Han, Y. Li, Inorg. Chem. Commun. 22 (2012) 73–76.
[62] C.X.A. Silva, V.L.C. Goncalves, C.J.A. Mota, Green Chem. 11 (2009) 38–41.
[63] J. Deutsch, A. Martin, H. Lieske, J. Catal. 245 (2007) 428–435.
[64] A.L. Maksimov, A.I. Nekhaev, D.S. Shlyakhtitsev, S.D. Varfolomeev, V.B. Vol'eva, G.A. Nikiforov, Pet. Chem. 50 (2010) 325–331.
[65] A.L. Maksimov, A.I. Nekhaev, D.N. Ramazanov, Yu.A. Arinicheva, A.A. Dzyubenko, S.N. Khadzhiev, Pet. Chem. 50 (2011) 61–69.
[66] W. Kantlehner, H.D. Gutbrod, B. Funke, Liebigs Ann. Chem. 2 (1980) 246–252.
[67] I. Barabas, I.-A. Todorut, Energy Fuels 25 (2011) 5767–5774.
[68] M.E. Tat, J.H. Van Gerpen, Measurement of Biodiesel Speed of Sound and its Impact on Injection Timing Final Report, Report 4 in a Series of 6, Department of Mechanical Engineering, Iowa State University, Ames, IA, USA, 2003 NREL/SR 510-31462, February.
[69] G. Knothe, Energy Environ. Sci. 2 (2009) 759–766.